Journal of Sound and Vibration (1999) **224**(2), 329–348
Article No. jsvi.1999.2171, available online at http://www.idealibrary.com on IDEAL®

A DOUBLE TIMOSHENKO BEAM MODEL FOR VERTICAL VIBRATION ANALYSIS OF RAILWAY TRACK AT HIGH FREQUENCIES

T. X. Wu*

Department of Mechanical Engineering, Shanghai Tiedao University, Shanghai 200331, *People's Republic of China*

AND

D. J. Thompson

*Institute of Sound and Vibration Research, University of Southampton, Southampton SO*17 1*BJ, England*

(*Received* 19 *October* 1998, *and in final form* 1 *February* 1999)

Models of track vibration representing the rail as a beam are insufficiently detailed for high frequencies where the rail cross-sectional deformation is significant. A double Timoshenko beam model is developed for vertical vibration analysis at high frequencies. Although simple, this model includes the essential cross-sectional deformation of a rail in vertical vibration at high frequencies. Based on this model, the dispersion relation of propagating waves in a free and a continuously supported rail is studied. Vertical vibration receptances of the rail are calculated using both continuously and discretely supported models. The results show good agreement with an FE model and measurement data in terms of frequency–wavenumber curves, point receptance and vibration decay rate.

1. INTRODUCTION

Models of the dynamic behaviour of track are required, amongst other things, for predicting the noise emitted as a train passes. For such applications, frequencies up to at least 5 kHz have to be considered [1]. It is more difficult to study the dynamic behaviour of railway track at high frequencies than at low frequencies because the cross-sectional deformation of the rail appears in high frequency vibration. Simple beam models [2, 3] cannot represent the cross-sectional deformation and thus are not appropriate to investigate high frequency vibration of railway track. Some theoretical models were developed by Scholl [4–6] for the analysis of dispersion relations in a free rail and allow

*Currently on leave at ISVR, University of Southampton, England

0022–460X/99/270329 + 20 $30.00/0

consideration of rail foot and rail web deformations. Advanced models based on the finite element method (FEM) or a derivative [7–12] have been developed for analysing high frequency vibration properties of railway track. Most of them are complicated models and thus numerical treatment is essential. For identifying the wavenumber–frequency relation in a free rail, FE models are straightforward. However, it is very time consuming to calculate high frequency responses of the rail to external excitation using FE models, especially when the discrete supports of the rail are taken into account, because a large number of degrees of freedom have to be included.

This may be improved by using some simplified rail models if such models can properly represent the corresponding cross-sectional deformations. As the vertical and lateral vibration behaviour of a rail are effectively uncoupled from each other due to symmetry and are affected by different properties of the cross-section, it is reasonable to study separately vertical and lateral vibration of a rail by different simplified models. In this paper only vertical vibration is taken into account. The lateral vibration of a rail is studied in reference [13] by using a multiple Timoshenko beam model. In principle, a simplified rail model for high frequency vertical vibration should allow the rail foot deformation of the cross-section. Based on this, a double Timoshenko beam model is developed, with one beam representing the rail head and web and another beam representing the rail foot. They are connected by an elastic component. At low frequencies the two beams vibrate together in the same way as a single Timoshenko beam, whereas at high frequencies a relative motion between the two beams appears, which represents the cross-sectional deformation between the rail head (and web) and foot.

Several aspects of the vertical vibration behaviour of railway track are investigated using the double beam model. Firstly, the dispersion relation of waves in a free and a continuously supported rail is explored, and then the point receptances of a continuously supported rail are studied. Lastly, the same analysis of the point receptances is carried out but for a discretely supported rail. Comparison with an FE model shows good agreement in terms of the frequency–wavenumber relation. Again good agreement with measurement data is reached in terms of both point receptance and vibration decay.

2. DOUBLE BEAM MODEL OF RAIL

The essential cross-sectional deformation of vertical vibration of a rail at high frequencies consists of foot flapping [8] (foot bending as a cantilever). A simplified rail model for high frequency vertical vibration should allow this type of cross-sectional deformation. The double beam model is schematically shown in Figure 1. The rail is divided into two parts: the upper part representing the head (and web), the lower part representing the foot. Although the foot has two branches, they may be combined together due to symmetry. Both the head and the foot are represented by infinite Timoshenko beams in the rail axis direction. These two beams are connected by continuously distributed springs to allow relative motion between them, which represents the foot flapping. In fact the rail

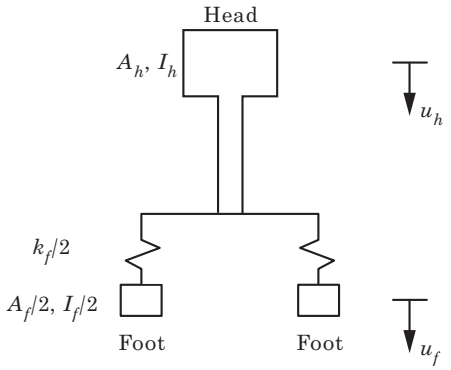

Figure 1. Cross-section of the double beam model of rail.

foot cross-section may be regarded as a cantilever beam. If considering the first order vibration mode only, this cantilever beam can be simplified to a single-degree-of-freedom (SDOF) system. The cross-section of the double beam model is just a SDOF system (rigid body motion excluded), thus the cross-sectional deformation–foot flapping can be represented by this model. It remains to be shown whether appropriate parameters can be found which allow this model to represent a rail across the required frequency range.

The material properties of the model are represented by E, the Young's modulus, G, the shear modulus and ρ, the density. The geometric properties of each cross-section are characterised by A, the cross-sectional area, I, the area moment of inertia and κ, the shear coefficient. The subscripts h and f are used to represent the rail head and foot respectively. k_f represents the equivalent stiffness (per unit length) for foot flapping. Applying Newton's second law of motion to the upper Timoshenko beam (the rail head and web) gives

$$\rho A_h \ddot{u}_h + G A_h \kappa_h (\Phi_h' - u_h'') + k_f (u_h - u_f) = 0, \tag{1}$$

$$\rho I_h \ddot{\Phi}_h + G A_h \kappa_h (\Phi_h - u_h') - E I_h \Phi_h'' = 0, \tag{2}$$

where u represents the transverse (vertical) motion of the beams, Φ the rotation of the cross-sections and $'$ indicates the derivative with respect to z. Similar equations can be written for the lower Timoshenko beam (the rail foot). Combining these equations gives

$$\mathbf{M}\ddot{\mathbf{q}} - \mathbf{D}\mathbf{q}'' - \mathbf{G}\mathbf{q}' + \mathbf{K}_R\mathbf{q} = \mathbf{0}, \tag{3}$$

where

$$\mathbf{M} = \rho \begin{bmatrix} A_h & & & \\ & I_h & & \\ & & A_f & \\ & & & I_f \end{bmatrix}, \qquad \mathbf{D} = \begin{bmatrix} G A_h \kappa_h & & & \\ & E I_h & & \\ & & G A_f \kappa_f & \\ & & & E I_f \end{bmatrix}, \tag{4, 5}$$

$$\mathbf{G} = \begin{bmatrix} 0 & -GA_h\kappa_h & & \\ GA_h\kappa_h & 0 & & \\ & & 0 & -GA_f\kappa_f \\ & & GA_f\kappa_f & 0 \end{bmatrix}, \tag{6}$$

$$\mathbf{K}_R = \begin{bmatrix} k_f & 0 & -k_f & 0 \\ 0 & GA_h\kappa_h & 0 & 0 \\ -k_f & 0 & k_f & 0 \\ 0 & 0 & 0 & GA_f\kappa_f \end{bmatrix}, \tag{7}$$

$$\mathbf{q} = (q_1 \quad q_2 \quad q_3 \quad q_4)^{\mathrm{T}} = (u_h \quad \Phi_h \quad u_f \quad \Phi_f)^{\mathrm{T}}. \tag{8}$$

To use the double beam model an important aspect is to determine the cross-sectional parameters. The foot area, A_f, is an equivalent value related to the first order frequency of foot flapping (cantilever beam bending, from the view of the cross-section). The equivalent mass of a uniform cantilever beam at its free end in its first bending mode of vibration is equal to $(33/140)m$, which can be obtained using Rayleigh's method and assuming the static deflections of the beam as its first vibration mode. Here m is the mass of the whole cantilever beam. The rail foot corresponds to approximately one third of the rail cross-sectional area. Thus A_f is roughly equal to $0.08A_r$, where A_r represents the rail cross-section area. The equivalent stiffness k_f is determined according to the foot flapping cut-on frequency. This frequency can be found by using a two-dimensional FE model of the cross-section. This is much simpler than the FE models for the whole rail considered in references [7–12]. The foot flapping cut-on frequency also can be determined by an experimental approach. The foot area moment of inertia, I_f, is with respect to the local neutral axis of the foot cross-section, so it is small and thus the head area moment of inertia, I_h, is approximately equal to the whole rail cross-sectional area moment of inertia. The head area, A_h, is equal to $A_r - A_f$. In this paper UIC 60 rail is chosen as an example. According to the principles listed above, the following parameters have been derived for use in calculations: $E = 2{\cdot}1 \times 10^{11}$ N/m^2; $G = 0{\cdot}77 \times 10^{11}$ N/m^2; $\rho = 7850$ kg/m^3; $A_h = 7{\cdot}09 \times 10^{-3}$ m^2; $I_h = 30{\cdot}40 \times 10^{-6}$ m^4; $\kappa_h = 0{\cdot}45$; $A_f = 0{\cdot}60 \times 10^{-3}$ m^2; $I_f = 0{\cdot}118 \times 10^{-6}$ m^4; $\kappa_f = 0{\cdot}85$; $k_f = 5{\cdot}33 \times 10^9$ N/m^2. A_f and k_f correspond to a foot flapping cut-on frequency of about 5600 Hz.

3. PROPAGATING WAVES IN FREE RAIL

3.1. EQUATION OF DISPERSION RELATION

Assuming the displacement vector $\mathbf{q}$ has the form of

$$\mathbf{q} = \mathbf{q}(z)\mathrm{e}^{\mathrm{i}\omega t}, \tag{9}$$

where

$$\mathbf{q}(z) = (u_h(z) \quad \Phi_h(z) \quad u_f(z) \quad \Phi_f(z))^{\mathrm{T}}, \tag{10}$$

and substituting (9) into equation (3) and taking derivatives with respect to time only, the results are given by

$$\mathbf{D}\mathbf{q}''(z) + \mathbf{G}\mathbf{q}'(z) + (\omega^2\mathbf{M} - \mathbf{K}_R)\mathbf{q}(z) = \mathbf{0}. \tag{11}$$

Taking $\mathbf{q}(z) = \mathbf{Q}\mathrm{e}^{-\mathrm{i}kz}$ and substituting it into (11) gives

$$[-k^2\mathbf{D} - \mathrm{i}k\mathbf{G} + (\omega^2\mathbf{M} - \mathbf{K}_R)]\mathbf{Q} = \mathbf{0}. \tag{12}$$

This is a quadratic eigenvalue problem. Since the matrices are of dimension 4×4, there are eight solutions for k at each frequency ω, four of which apply to each direction. The solutions for wavenumber k at a given frequency ω are usually complex and have the form of $k = \pm(a \pm \mathrm{i}b)$, where a and b are real. They appear in opposite pairs when k is purely real or purely imaginary or in double pairs when k is complex. The imaginary part b represents the wave decay. When $b = 0$, the wave is propagating. The eigenvector $\mathbf{Q}$ represents the wave shapes and it is also complex. When $k = 0$, equation (12) becomes

$$(\omega^2\mathbf{M} - \mathbf{K}_R)\mathbf{Q} = \mathbf{0}. \tag{13}$$

Then the cut-on frequencies can be obtained from (13). At a cut-on frequency each cross-section in the rail vibrates in phase over the whole length.

To solve the quadratic eigenvalue problem, it is appropriate to convert equation (11) into the state space form. Taking

$$\mathbf{X} = \begin{bmatrix} \mathbf{q}(z) \\ \mathbf{q}'(z) \end{bmatrix}, \quad \mathbf{A} = \begin{bmatrix} \mathbf{0} & \mathbf{I} \\ -\mathbf{D}^{-1}(\omega^2\mathbf{M} - \mathbf{K}_R) & -\mathbf{D}^{-1}\mathbf{G} \end{bmatrix}, \tag{14, 15}$$

equation (11) can be written in the state space form:

$$\mathbf{X}' = \mathbf{A}\mathbf{X}. \tag{16}$$

This leads to a normal eigenvalue problem

$$\det(\lambda\mathbf{I} - \mathbf{A}) = 0, \tag{17}$$

where $\lambda = -\mathrm{i}k$. From equation (17) the dispersion relation of propagating waves in the rail can be determined.

3.2. WAVES IN A FREE RAIL

To validate the double beam model a 3-D FE model representing UIC 60 rail is also used. The FE mesh of the rail cross-section is shown in Figure 2. It is a short length of rail (1 m) with symmetrical or antisymmetrical boundary conditions at the ends to simulate the waves in an infinite rail. Calculations are carried out using ANSYS with 3-D linear solid elements. The results from the double beam model and FE model are shown in Figure 3. Two waves are extracted from the FE model for comparison, whereas three propagating waves are predicted by the simplified model in the frequency region studied. In fact

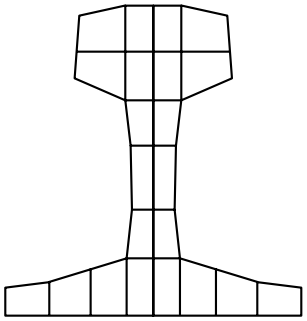

Figure 2. FE mesh of cross-section of UIC 60 rail (3-D FE model).

there are four waves in each direction according to equation (12), but one of them, the cross-sectional rotation of the first beam, only becomes propagating at very high frequencies (above 32 kHz). Wave I represents vertical bending at low wavenumbers, but involving foot flapping at high wavenumbers. Wave II is characterised by foot flapping. In the double beam model this wave starts at a lower frequency and initially features cross-sectional rotation of the second Timoshenko beam representing the foot. Wave III starts as foot flapping and then transfers to the cross-sectional rotation of the second beam. A significant deviation for wave I between the simplified model and FE model can be seen starting at about 5000 Hz. This is not critical, however, because the foot flapping characteristic wave becomes dominant in the response of a rail above this frequency. Thus the simplified model is expected to give satisfactory results in later calculations. For comparison, the result from a single Timoshenko beam model is also included in Figure 3. The wavenumber in the single Timoshenko beam can be seen to be very close to the wave I of the double beam model, but in the single Timoshenko beam model the whole cross-section of a rail vibrates in the same way and there is no cross-sectional deformation at all.

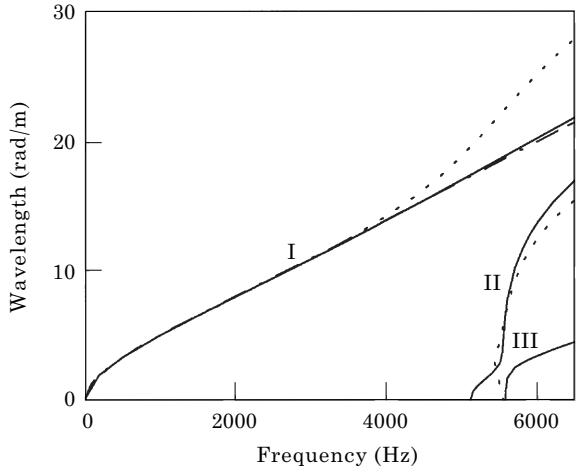

Figure 3. Dispersion relation of waves in a free rail for vertical vibration: ——, from the double beam model; ·····, from the 3-D FE model; –·–·–, from the single Timoshenko beam model.

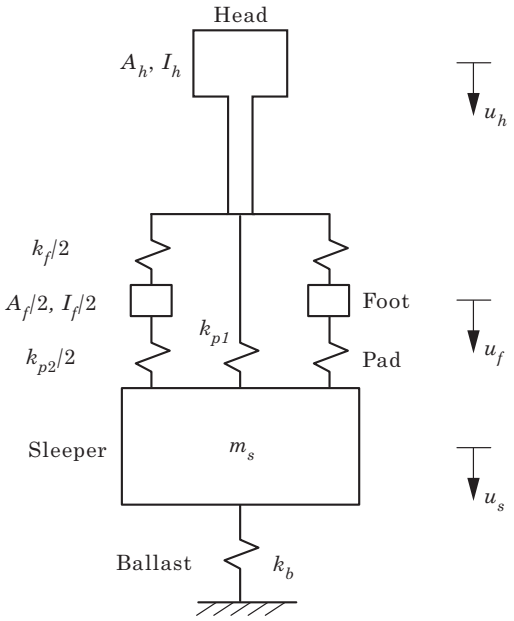

Figure 4. Cross-section of continuously supported rail.

4. CONTINUOUSLY SUPPORTED RAIL MODEL

Although a realistic rail is discretely supported by pads and sleepers, a continuously supported rail model can be used to explore the basic dynamic properties of a railway track without involving the complication of the periodic support. In this section a continuously supported rail model is employed to calculate the dispersion relation of waves in the rail and the receptances of the rail. The pad, sleeper and the ballast are represented by equivalent continuous layers of mass and stiffness. The parameters of these layers and the rail are the same as in the previous sections.

4.1. WAVES IN CONTINUOUSLY SUPPORTED RAIL

The continuously supported rail model is schematically shown in Figure 4, where the pad stiffness k_p is split into two components: $k_p = k_{p1} + k_{p2}$, with k_{p1} acting beneath the centre of the rail and k_{p2} beneath the foot, and taking $k_{p1} = k_{p2}$. m_s and k_b represent sleeper mass and ballast stiffness respectively. In the rest of the paper, it will be assumed that forces and responses are harmonic, so the $e^{i\omega t}$ term will usually be omitted. The equation of motion for the continuously supported rail is

$$-\mathbf{D}\mathbf{q}''(z) - \mathbf{G}\mathbf{q}'(z) - (\omega^2\mathbf{M} - \mathbf{K}_R)\mathbf{q}(z) = (-k_{p1}(u_h - u_s) \quad 0 \quad -k_{p2}(u_f - u_s) \quad 0)^{\mathrm{T}}, \tag{18a}$$

and for the sleeper

$$-m_s\omega^2 u_s = -k_{p1}(u_s - u_h) - k_{p2}(u_s - u_f) - k_b u_s. \tag{18b}$$

From (18b) u_s can be written as follows:

$$u_s = (k_{p1}u_h + k_{p2}u_f)/(k_p + k_b - m_s\omega^2). \tag{19}$$

Substituting (19) into (18a) gives

$$\begin{aligned} &-\mathbf{D}\mathbf{q}''(z) - \mathbf{G}\mathbf{q}'(z) - (\omega^2\mathbf{M} - \mathbf{K}_R)\mathbf{q}(z) \\ &\quad = (-Z_{11}u_h - Z_{13}u_f \quad 0 \quad -Z_{31}u_h - Z_{33}u_f \quad 0)^{\mathrm{T}}, \end{aligned} \tag{20}$$

where Z_{11}, Z_{13}, Z_{31} and Z_{33} are the dynamic stiffnesses of the continuous foundation:

$$Z_{11} = k_{p1}(k_{p2} + k_b - m_s\omega^2)/(k_p + k_b - m_s\omega^2), \tag{21a}$$

$$Z_{33} = k_{p2}(k_{p1} + k_b - m_s\omega^2)/(k_p + k_b - m_s\omega^2), \tag{21b}$$

$$Z_{13} = Z_{31} = -k_{p1}k_{p2}/(k_p + k_b - m_s\omega^2). \tag{21c}$$

Thus equation (18) can be simplified to

$$\mathbf{D}\mathbf{q}''(z) + \mathbf{G}\mathbf{q}'(z) + (\omega^2\mathbf{M} - \mathbf{K})\mathbf{q}(z) = \mathbf{0}, \tag{22}$$

where

$$\mathbf{K} = \mathbf{K}_R + \begin{bmatrix} Z_{11} & 0 & Z_{13} & 0 \\ 0 & 0 & 0 & 0 \\ Z_{31} & 0 & Z_{33} & 0 \\ 0 & 0 & 0 & 0 \end{bmatrix}. \tag{23}$$

To calculate the frequency–wavenumber relation in a supported rail, the following parameters of the track foundation are used which are based on values from reference [14] for track C: $k_p = 583{\cdot}3$ MN/m^2; $k_b = 83{\cdot}3$ MN/m^2; $m_s = 270$ kg/m.

The frequency–wavenumber relation in the supported rail can be seen from Figure 5 to be almost the same as in the free rail except wave I at low frequencies. There is a branch for this vertical bending wave I at about 80–250 Hz. In this frequency region the rail vibration is coupled with the foundation mass. In the higher frequency region the wavenumber–frequency relation of waves I, II and III are the same as in the free rail.

For a realistic railway track, damping should be taken into consideration. It can be added by means of a loss factor to the pad and ballast stiffnesses to make them complex. Here $\eta_p = 0{\cdot}25$ and $\eta_b = 1{\cdot}0$ are taken for the pad and ballast respectively. No damping is added to the rail. Damping will make the wavenumber k always complex with the form of $k = \pm(a - \mathrm{i}b)$, which represent two waves propagating in opposite directions with exponential decay. The decay rate Δ (in dB/m) of various waves is determined by their imaginary part of k and can be calculated using

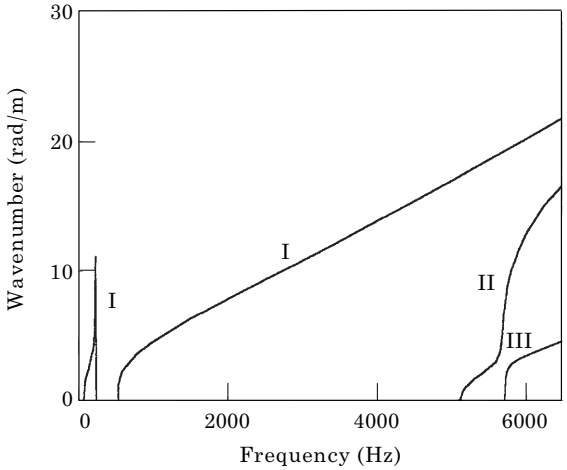

Figure 5. Dispersion relation of waves in a continuously supported rail without damping for vertical vibration.

$$\Delta = 20 \log_{10}(e^b) = 8{\cdot}686b. \tag{24}$$

The frequency–wavenumber relation in a supported rail with damping is shown in Figure 6 where the solid lines represent the real part of the wavenumber and the dotted lines the imaginary part. The curves of the real part can be seen to be similar to the case of no damping, apart from near the cut-on frequencies. The wave of cross-sectional rotation of the foot forms a single curve in Figure 6, whereas in Figure 5 this wave is separated in waves II and III. The imaginary parts can be seen to be higher near the cut-on frequencies and much lower thereafter. The decay rates of various waves in Figure 7 show this more noticeably. They can be seen to decrease dramatically after the cut-on frequencies.

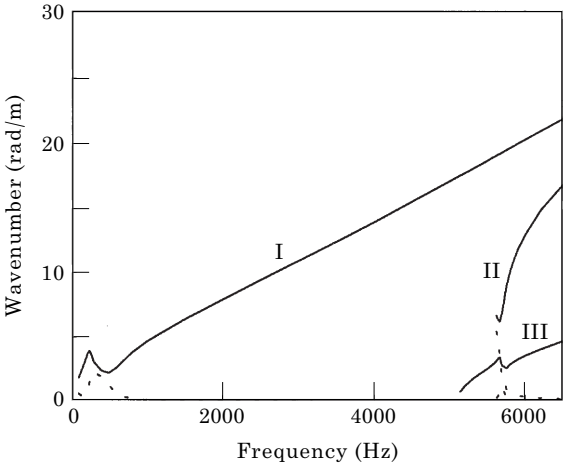

Figure 6. Dispersion relation of waves in a continuously supported rail with damping for vertical vibration: ——, real part of the wavenumber; ·····, imaginary part of the wavenumber.

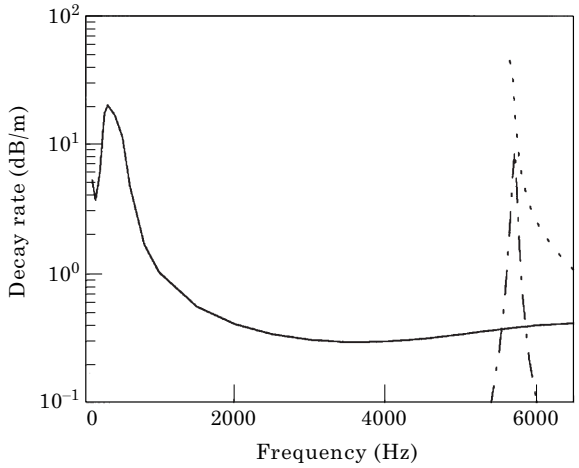

Figure 7. Decay rates of different waves in a continuously supported rail: ——, wave I, –·–·–, wave II; ·····, wave III.

4.2. RECEPTANCES

Supposing a harmonic external force $Fe^{i\omega t}$ acting on the rail head at $z = 0$, the equation of motion is given as:

$$-\mathbf{D}\mathbf{q}''(z) - \mathbf{G}\mathbf{q}'(z) - (\omega^2\mathbf{M} - \mathbf{K})\mathbf{q}(z) = (F\delta(z) \quad 0 \quad 0 \quad 0)^{\mathrm{T}}. \tag{25}$$

Equation (25) can be written in the state space form:

$$\mathbf{X}' = \mathbf{A}\mathbf{X} + \mathbf{P}\delta(z), \tag{26}$$

where $\mathbf{A}$ has the same form as in equation (15) but $\mathbf{K}_R$ is replaced by $\mathbf{K}$ which is the sum of rail stiffness matrix $\mathbf{K}_R$ and foundation dynamic stiffness matrix, see equation (23), and

$$\mathbf{P} = [\mathbf{0} \quad -\mathbf{D}^{-1}\mathbf{F}]^{\mathrm{T}}, \quad \mathbf{F} = (F \quad 0 \quad 0 \quad 0)^{\mathrm{T}}. \tag{27a, b}$$

Taking the Laplace transform of equation (26) gives

$$(s\mathbf{I} - \mathbf{A})\mathbf{X}(s) = \mathbf{P}. \tag{28}$$

The Laplace transform of the rail head and foot displacements, respectively, has the form of

$$U_h(s) = \Delta_1(s)/\Delta(s), \quad U_f(s) = \Delta_3(s)/\Delta(s), \tag{29, 30}$$

where, $\Delta(s)$ is the determinant of matrix $(s\mathbf{I} - \mathbf{A})$. $\Delta_1(s)$ and $\Delta_3(s)$ are the determinants of the matrices which are obtained from $(s\mathbf{I} - \mathbf{A})$ by replacing its first column and third column by $\mathbf{P}$ respectively. The vertical responses of the rail head and foot are found by performing the Laplace inverse transform using contour integration:

$$u_h(z) = \frac{1}{2\pi i}\int_{\gamma-i\infty}^{\gamma+i\infty} U_h(s)e^{sz}\,ds = \sum_{\substack{k \text{ with } \mathrm{Re}(s_k)<0 \text{ or} \\ \mathrm{Im}(s_k)<0 \text{ if } \mathrm{Re}(s_k)=0}} \mathrm{Res}[U_h(s_k)e^{s_k z}], \quad z > 0; \tag{31}$$

$$u_f(z) = \frac{1}{2\pi i}\int_{\gamma-i\infty}^{\gamma+i\infty} U_f(s)e^{sz}\,ds = \sum_{\substack{k \text{ with } \mathrm{Re}(s_k)<0 \text{ or} \\ \mathrm{Im}(s_k)<0 \text{ if } \mathrm{Re}(s_k)=0}} \mathrm{Res}[U_f(s_k)e^{s_k z}], \quad z > 0; \tag{32}$$

where the residues at the poles s_k are given by

$$\mathrm{Res}[U_h(s_k)e^{s_k z}] = [\Delta_1(s_k)/\Delta'(s_k)]e^{s_k z}, \quad \mathrm{Res}[U_f(s_k)e^{s_k z}] = [\Delta_3(s_k)/\Delta'(s_k)]e^{s_k z}. \tag{33, 34}$$

The responses of the rail head and foot at $z = 0$ to a unit harmonic excitation at the same point are shown in Figure 8 in terms of amplitude and phase. Three resonance peaks can be seen at about 80 Hz, 520 Hz and 5600 Hz. At 80 Hz the whole track bounces on the vertical stiffness of the ballast, while at 520 Hz the rail vibrates on the pad stiffness. These two peaks can be regarded as the cut-on of the vertical bending wave (two branches, see Figure 5), and the peak at 5600 Hz is due to the cut-on of the foot flapping. The foot response can be

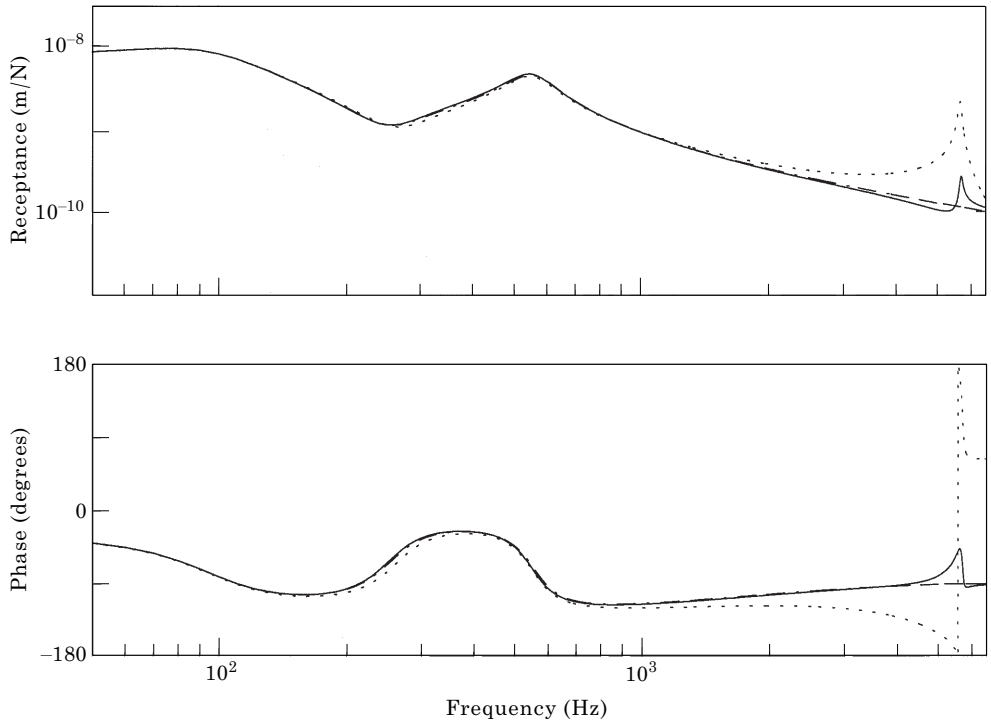

Figure 8. Amplitude and phase of the point receptance (head response) and foot response of the continuously supported rail for vertical vibration: ——, head response; ·····, foot response, –·–·–, point receptance of the single Timoshenko beam model.

observed to be very similar to the head response below 2000 Hz, whereas at high frequencies it is much higher than the head response, up to a factor 10. At the peak area near the foot flapping cut-on frequency the foot response can be seen to be very sharp and out of phase with the head. Comparing all these results with those in reference [8], which shows the same trends from a more complex model, one can see that the vertical vibration properties of a rail at high frequencies are very well predicted using the double Timoshenko beam model. The result from a single Timoshenko beam model is also shown in Figure 8. The point receptance of the single beam model can be seen to be almost the same as the head response of the double beam model except for the peak at the foot flapping cut-on frequency. Therefore, a conventional beam model may be used for vertical vibration very well up to about 2000 Hz, but above this up to about 5000 Hz such a model may only be used for predicting the head response because at high frequencies the deviation between the head and foot response becomes more and more significant. Moreover, the decay rate of the vertical bending wave can be seen in Figure 7 to stabilise around 0·4 dB/m whereas the result for a single Timoshenko beam is continuous to fall at high frequencies (refer to Figure 13). The higher decay rate found with the double beam model, which corresponds qualitatively to that found in reference [8], is due to the higher amplitudes of vibration on the foot acting on the rail pad.

5. DISCRETELY SUPPORTED RAIL MODEL

A more realistic model for railway track should be an infinite rail with periodic supports. Such a model will introduce the complication of the periodic support nature and thus difficulties in dealing with it, but some important characteristics, for example, pinned–pinned resonances can only be obtained using a discretely supported model. In this section the complication of the discretely supported model is addressed using Green's function and the superposition principle.

5.1. EQUATION OF MOTION

An infinite periodically supported rail model is shown in Figure 9. The supports are characterised by pad stiffnesses, K_{pn}, sleeper mass, M_s and ballast

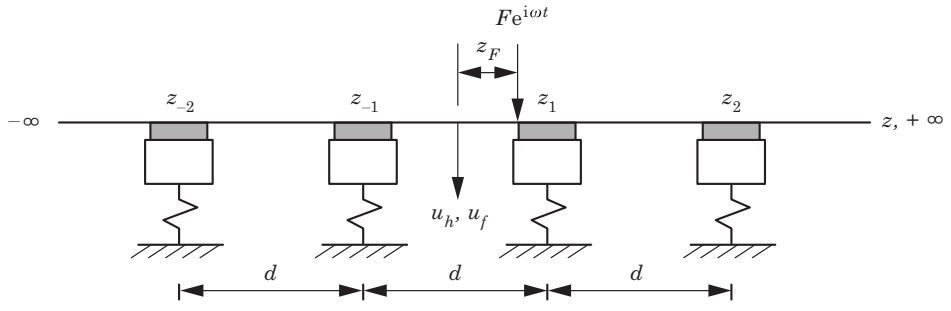

Figure 9. Discretely supported rail model.

stiffness, K_{bn}. The pad stiffness K_{pn} is also split into two components as in the continuously supported model: $K_{pn} = K_{pn1} + K_{pn2}$, with K_{pn1} acting beneath the centre of the rail and K_{pn2} beneath the foot, and taking $K_{pn1} = K_{pn2}$. Damping is considered by introducing loss factors η_r into the Young's modulus E and shear modulus G of the rail and the equivalent stiffness k_f of foot flapping, η_p into the pad stiffnesses K_{pn}, η_b into the ballast stiffness K_{bn}, and making E, G, k_f, K_{pn}, and K_{bn} complex with the appropriate factor $(1 + i\eta)$. In fact the rail damping is very small, usually less than 0·0001. The main reason for adding extra damping to the rail is to suppress the pinned–pinned resonance peaks on which the track foundation damping has very little effect. In reality, the pinned–pinned resonance peaks are not as sharp as in theoretical analysis because of the variable sleeper spacing and the distributed contact between the rail and pads. In the theoretical model, however, the sleeper spacing is chosen as constant and the rail is assumed as ideally point-supported. Assuming the nth support is at the position $z = z_n$ and a single external harmonic force $Fe^{i\omega t}$ acts on the rail head at $z = z_F$, the equation of motion of the discretely supported rail is given as

$$-\mathbf{D}\mathbf{q}''(z) - \mathbf{G}\mathbf{q}'(z) - (\omega^2\mathbf{M} - \mathbf{K}_R)\mathbf{q}(z) = (F\delta(z - z_F) + F_1 \quad 0 \quad F_3 \quad 0)^{\mathrm{T}}, \tag{35}$$

where

$$F_1 = -\sum_{\substack{n=-\infty \\ n\neq 0}}^{\infty} [Z_{11n}u_h(z_n) + Z_{13n}u_f(z_n)]\delta(z - z_n), \tag{36a}$$

$$F_3 = -\sum_{\substack{n=-\infty \\ n\neq 0}}^{\infty} [Z_{31n}u_h(z_n) + Z_{33n}u_f(z_n)]\delta(z - z_n), \tag{36b}$$

where Z_{11n}, Z_{13n}, Z_{31n} and Z_{33n} are the dynamic stiffnesses at nth support:

$$Z_{11n} = K_{p1n}(K_{p2n} + K_{bn} - M_s\omega^2)/(K_{pn} + K_{bn} - M_s\omega^2), \tag{37a}$$

$$Z_{33n} = K_{p2n}(K_{p1n} + K_{bn} - M_s\omega^2)/(K_{pn} + K_{bn} - M_s\omega^2), \tag{37b}$$

$$Z_{13n} = Z_{31n} = -K_{p1n}K_{p2n}/(K_{pn} + K_{bn} - M_s\omega^2). \tag{37c}$$

5.2. RESPONSE OF THE DISCRETELY SUPPORTED RAIL

The discretely supported track model can be treated in various ways. One approach is developed by Heckl [15], see also reference [16]. In this approach, the discrete rail supports are replaced by corresponding external forces, and thus the railway track can be simply considered as an infinite beam with many point forces acting on it. Based on the Green's function and the superposition principle the stationary response of the rail to the harmonic excitation can be obtained. In addition the infinite beam is modelled with a finite number of supports, the number being chosen large enough to guarantee a reliable

approximate solution. This approach is also employed here, but now for the double beam model Green's function matrices have to be used instead of a single Green's function. Moreover the symmetry of the railway track about the forcing point for excitation above a sleeper or at mid-span is taken into account to increase the efficiency of the calculation.

The Green's function $g_{ij}(z, z')$ is defined as the response at z of the ith component of the displacement vector $\mathbf{q}(z)$ caused by a unit harmonic force at z' which is the jth component of the excitation vector **F.** It can be obtained by applying a similar method as used in section 4, but now to a free rail instead of the continuously supported rail and with the force and response positions at different values of z.

Using the superposition principle the displacements of the rail head and foot are given by

$$u_h(z) = -\sum_{\substack{n=-N \\ n\neq 0}}^{N} \{[Z_{11n}u_h(z_n) + Z_{13n}u_f(z_n)]g_{11}(z, z_n) + [Z_{31n}u_h(z_n) + Z_{33n}u_f(z_n)]g_{13}(z, z_n)\} + Fg_{11}(z, z_F); \tag{38a}$$

$$u_f(z) = -\sum_{\substack{n=-N \\ n\neq 0}}^{N} \{[Z_{11n}u_h(z_n) + Z_{13n}u_f(z_n)]g_{31}(z, z_n) + [Z_{31n}u_h(z_n) + Z_{33n}u_f(z_n)]g_{33}(z, z_n)\} + Fg_{31}(z, z_F); \tag{38b}$$

or in matrix form

$$\begin{pmatrix} u_h(z) \\ u_f(z) \end{pmatrix} = -\sum_{\substack{n=-N \\ n\neq 0}}^{N} \begin{bmatrix} Z_{11n}g_{11}(z, z_n) + Z_{31n}g_{13}(z, z_n) & Z_{13n}g_{11}(z, z_n) + Z_{33n}g_{13}(z, z_n) \\ Z_{11n}g_{31}(z, z_n) + Z_{31n}g_{33}(z, z_n) & Z_{13n}g_{31}(z, z_n) + Z_{33n}g_{33}(z, z_n) \end{bmatrix} \times \begin{pmatrix} u_h(z_n) \\ u_f(z_n) \end{pmatrix} + F\begin{pmatrix} g_{11}(z, z_F) \\ g_{31}(z, z_F) \end{pmatrix}. \tag{39}$$

Equation (39) can be presented in a compact form:

$$\mathbf{u}(z) = -\sum_{\substack{n=-N \\ n\neq 0}}^{N} \mathbf{G}_u(z, z_n)\mathbf{u}(z_n) + F\mathbf{G}_F(z, z_F). \tag{40}$$

If $Fe^{i\omega t}$ acts at mid-span ($z = 0$), the following symmetric relationship holds:

$$\mathbf{u}(z) = \mathbf{u}(-z), \quad Z_{ijn} = Z_{ij(-n)}, \quad g_{ij}(z, z') = g_{ij}(-z, -z'). \tag{41a, b, c}$$

Equation (40) can be simplified to

$$\mathbf{u}(z) = -\sum_{n=1}^{N} [\mathbf{G}_u(z, z_n) + \mathbf{G}_u(z, -z_n)]\mathbf{u}(z_n) + F\mathbf{G}_F(z, 0). \tag{42}$$

At each support point $z = z_m$ the displacements of the rail head and foot can be written as:

$$\mathbf{u}(z_m) = -\sum_{n=1}^{N}[\mathbf{G}_u(z_m, z_n) + \mathbf{G}_u(z_m, -z_n)]\mathbf{u}(z_n) + F\mathbf{G}_F(z_m, 0) \quad m = 1, 2, \ldots, N. \tag{43}$$

From equation (43) the displacements of the rail head and foot at each support point can be solved in terms of F by taking the sum to the left side and then inverting the matrix of coefficients of $\mathbf{u}(z_m)$. Substituting them into equation (42), displacements of the rail head and foot at any point can be obtained.

For $Fe^{i\omega t}$ acting above a sleeper (this sleeper is now chosen as $n = 0$ and also $z = 0$) the similar equations for the displacements of the rail head and foot can be given as follows:

$$\mathbf{u}(z) = -\mathbf{G}_u(z, 0)\mathbf{u}(0) - \sum_{n=1}^{N}[\mathbf{G}_u(z, z_n) + \mathbf{G}_u(z, -z_n)]\mathbf{u}(z_n) + F\mathbf{G}_F(z, 0), \tag{44}$$

$$\mathbf{u}(z_m) = -\mathbf{G}_u(z_m, 0)\mathbf{u}(0) - \sum_{n=1}^{N}[\mathbf{G}_u(z_m, z_n) + \mathbf{G}_u(z_m, -z_n)]\mathbf{u}(z_n) + F\mathbf{G}_F(z_m, 0)$$
$$m = 0, 1, 2, \ldots, N \tag{45}$$

In a similar way the displacements of the rail head and foot at each support point can be solved from equation (45). Substituting them into equation (44), displacements of the rail head and foot at any point can be obtained.

5.3. NUMERICAL RESULTS

The point receptance and the foot response at the forcing point are calculated in the frequency range 50–6500 Hz for a unit vertical excitation acting at the rail head either above a sleeper or at mid-span. Parameters for each support are uniform and chosen as follows (to correspond to those used earlier for the continuous support): $K_p = 350$ MN/m; $K_b = 50$ MN/m; $M_s = 162$ kg/m. Other parameters such as loss factors are the same as used in the previous sections. In addition damping is added to the rail with loss factor $\eta_r = 0{\cdot}01$. The span length (the distance between two sleepers) is chosen as $d = 0{\cdot}6$ m, and the number of supports $2N = 80$ for the excitation acting at mid-span, $2N + 1 = 81$ for the excitation acting above a sleeper.

The amplitude and phase of the point receptance are shown in Figure 10, and the corresponding amplitude of the foot response is shown in Figure 11. Some characteristic peaks or troughs are marked with numbers from 1 to 9 in Figures 10 and 11. In general the response at low frequencies up to about 800 Hz can be seen to be similar for the excitation either acting at mid-span or above a sleeper. At low frequencies the responses of the rail head are similar to those of the foot, but at high frequencies the foot responses are higher than the head responses. This observation has also been obtained from the continuously supported model

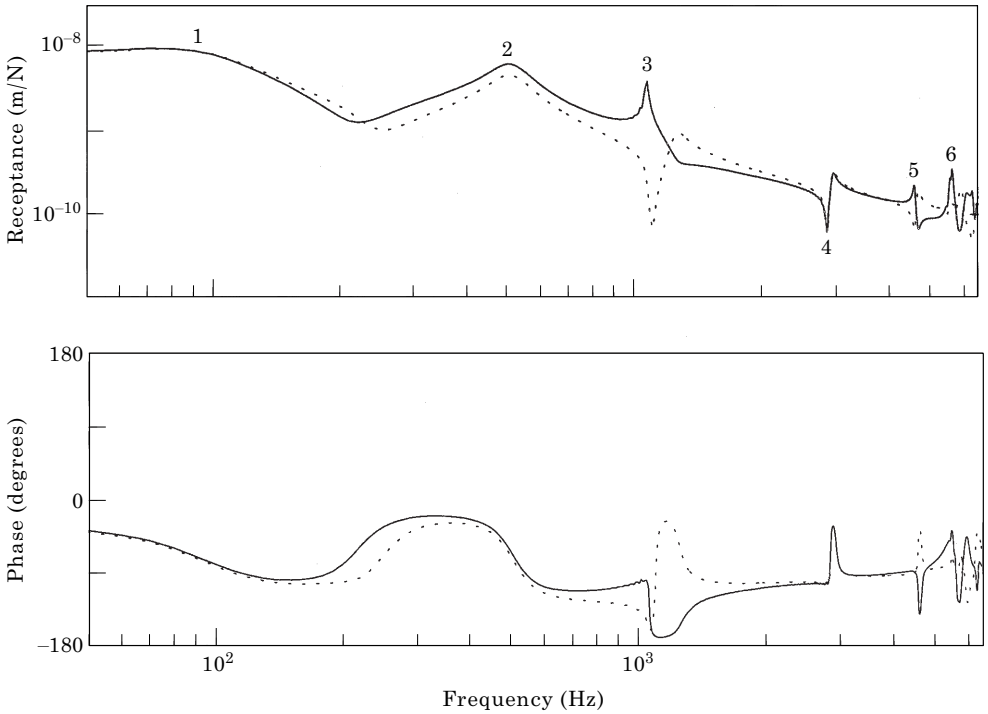

Figure 10. Amplitude and phase of the point receptance of the discretely supported rail for vertical vibration: ——, for excitation acting at mid-span; ·····, for excitation acting above a sleeper (for meaning of numbers see text).

(Figure 8). Two peaks at about 80 Hz and 520 Hz marked with 1 and 2 can be identified as the cut-on of the vertical bending wave (including its branch). Another peak at about 5600 Hz marked with 6 is the cut-on of the foot flapping. These three peaks are the same as those from the continuously supported model.

The main pinned–pinned resonance marked with 3 appears at about 1050 Hz. Here the vertical bending wavelength is equal to twice the span length and this

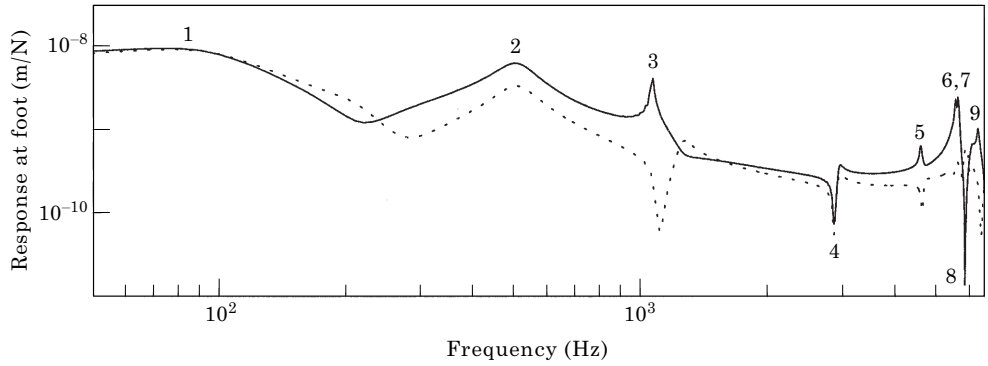

Figure 11. Vertical vibration amplitude of the foot response at forcing point: ——, for excitation acting at mid-span: ·····, for excitation acting above a sleeper (for meaning of numbers see text).

corresponds to a wavenumber of 5·2 rad/m in Figure 5. The third pinned–pinned resonance marked with 5 appears at about 4600 Hz when the vertical bending wavelength is equal to two thirds of the span length (corresponding to a wavenumber of 15·7 rad/m in Figure 5). The pinned–pinned resonances due to the foot flapping wave appear at much higher frequencies. They may be observed from the foot response in Figure 11, being marked with 7 and 9. When the wavelength is equal to the span length (corresponding to a wavenumber of 10·4 rad/m in Figure 5), the second pinned–pinned resonance occurs. However, for excitation at either mid-span or above a sleeper both the point receptances and the foot responses at the forcing point should be minimum. For the vertical bending wave the frequency corresponding to this minimum response is about 2800 Hz, whereas for the foot flapping it is about 5700 Hz. These two troughs are marked with 4 and 8 in Figures 10 and 11. All these properties related to the span length can only be observed using a discretely supported rail model and were not seen in Figure 8.

5.4. COMPARISON WITH MEASUREMENT DATA

Some experimental results are available in reference [14] and comparisons are made here with results from one track, track C, which had UIC 60 rail with concrete monobloc sleepers. The measurements were carried out on unloaded tracks by means of impact excitation using an instrumented hammer. For

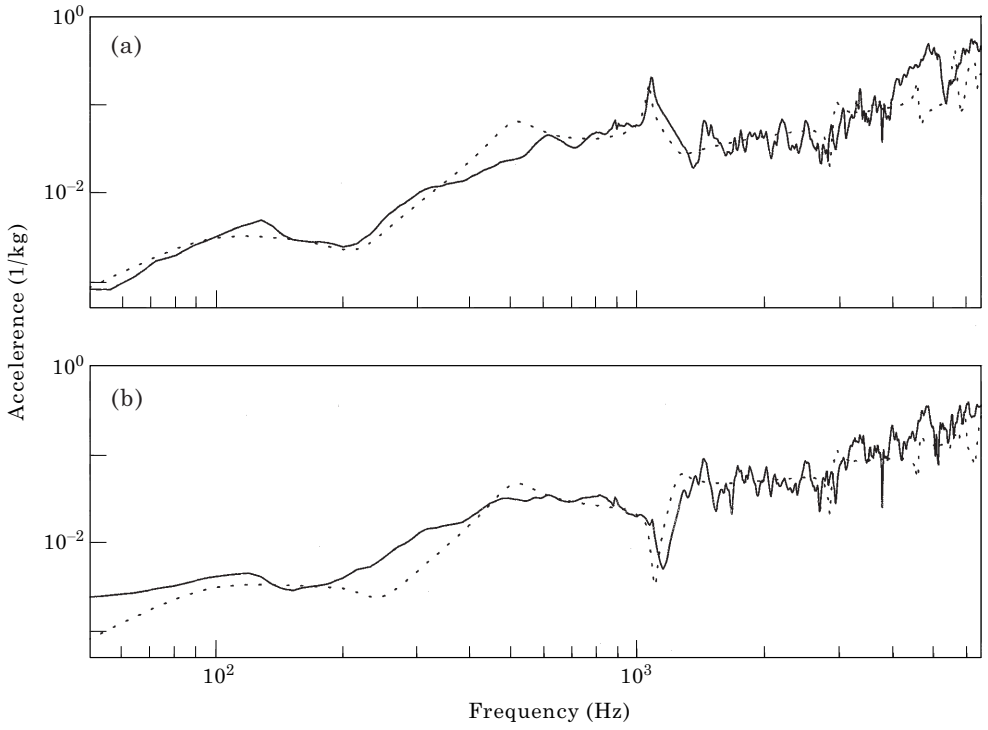

Figure 12. Comparison of predictions from the discretely supported double beam model and measurements: (a) excitation acting at mid-span; (b) excitation acting above a sleeper: ——, from measurements [14]; · · · · · ·, from predictions.

vertical vibration the excitation acted in the centre of the rail head and the response was obtained from the analogue sum of two acceleration signals on either side of the head. The measured and predicted vertical accelerances are compared in Figures 12(a) and 12(b) which are for the excitation acting at mid-span and above a sleeper respectively. The input parameters for the track are as in previous sections. A good agreement can be seen from Figure 12 in the whole frequency region, and especially in the region of 600–4000 Hz which is of most importance for noise radiation. The main deviations can be seen to occur near 500 Hz and in the region of 4000–5000 Hz for excitation at mid-span, and in the low frequency region up to about 500 Hz for excitation above a sleeper. The deviations in the low frequency region may be improved by considering the effect of sleeper vibration modes on the dynamic stiffness at the support point.

The decay rates of the vertical vibration along the rail from the continuous and periodic models are also compared with measurement data. For the continuous model the decay rate is represented by the imaginary part of the vertical bending wavenumber and calculated by equation (24). For the periodic model it is calculated from the attenuation in vibration level over a 25 span length from the excitation point divided by this distance (15 m). The measured decay rate is the average decay rate from the measurement in 1/3 octave bands. The comparison is shown in Figure 13. It can be seen that the tendency of the decay rates from the theoretical models is consistent with the measurement, that is, the vertical vibration decay is generally higher at low frequencies and lower at high frequencies. The periodic model gives a better result in the decay rate throughout the whole frequency region from 100–5000 Hz, whereas the decay rate from the continuous model without rail damping is underestimated at high frequencies but better than that of the single Timoshenko beam model. This is because the double beam model allows the foot flapping at high frequencies which results in more energy being dissipated through the damping in the track

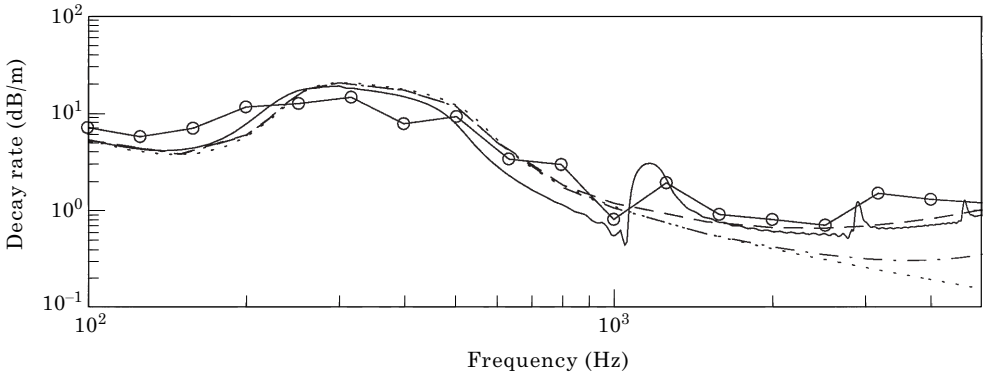

Figure 13. Decay rates of vertical vibration along the rail: ○—○, measured from [14]; ——, from the discretely supported double beam model; – – – –, from the continuously supported double beam model with rail damping ($\eta_r = 0{\cdot}01$); –·–·–, from the continuously supported double beam model without rail damping; ·····, from the continuously supported single Timoshenko beam model without rail damping.

foundation. The decay rate in the periodic model and continuous model with rail damping is further enhanced by the assignment of a loss factor (0·01) to the rail.

6. CONCLUSIONS

A double beam model has been presented for analysing the vertical vibration behaviour of railway track at high frequencies. This model is much simpler than the commonly used FE or FE based models and allows the essential cross-sectional deformation for the vertical vibration up to at least 6500 Hz. The dispersion relation of propagating waves in a free and a continuously supported rail has been studied. Vertical vibration receptances of the rail have been calculated using both continuously and discretely supported rail models. Comparison with an FE model has shown good agreement in terms of frequency–wavenumber relation. Good agreement with measurement data has also been reached in terms of point receptance and vibration decay rate along the rail.

The results show that the conventional Timoshenko beam model may be used only up to about 2000 Hz because the rail foot flapping occurs at high frequencies which leads to the foot response being considerably larger than that of the head at high frequencies, up to a factor 10 at about 5600 Hz. Compared with the continuously supported rail model, the predictions from the discretely supported rail model show that the track support has significant effects on the vertical vibration from about 1000 to 6500 Hz. Many peaks or troughs of the receptance appear in this frequency region. Since these peaks reach relatively high levels, neglecting them may cause significant errors. Thus the discretely supported rail model is more appropriate than the continuously supported model for vertical vibration.

REFERENCES

1. D. J. THOMPSON 1990 *Ph.D. Thesis, University of Southampton*. Wheel-rail noise: theoretical modelling of the generation of vibrations.
2. S. L. GRASSIE, R. W. GREGORY, D. HARRISON and K. L. JOHNSON 1982 *Journal Mechanical Engineering Science* **24**, 77–90. The dynamic response of railway track to high frequency vertical excitation.
3. MARIA HECKL 1991 *Report to the ORE Committee* C163. Acoustic behaviour of a periodically supported Timoshenko beam.
4. W. SCHOLL 1987 *VDI Fortschritt-Berichte*, Reihe 11, Nr. 93. Darstellungen des Körperschalls in Platten durch Übertragungsmatrizen und Anwendung auf die Berechnung der Schwingungsformen von Eisenbahnschienen.
5. W. SCHOLL 1982 *Acustica* **52**, 10–14. Schwingungsuntersuchung an Eisenbahn-schienen.
6. W. SCHOLL 1984 *Proceedings of the Second International Conference on Recent Advances in Structural Dynamics, Southampton* **II**, 699–707. Two theoretical models for wave propagation in rails.
7. B. RIPKE and K. KNOTHE 1991 *VDI Fortschritt-Berichte*, Reihe 11, Nr. 155. Die unendlich lange Schiene auf diskreten Schwellen bei harmonischer Einzellasterregung.

8. D. J. THOMPSON 1993 *Journal of Sound and Vibration* **161**, 421–446. Wheel–rail noise generation, part III: rail vibration.
9. KL KNOTHE, Z. STRZYZAKOWSKI and K. WILLNER 1994 *Journal of Sound and Vibration* **169**, 111–123. Rail vibrations in the high frequency range.
10. L. GAVRIC 1995 *Journal of Sound and Vibration* **185**, 531–543. Computation of propagating waves in free rail using a finite element technique.
11. L. GRY 1996 *Journal of Sound and Vibration* **195**, 477–505. Dynamic modelling of railway track based on wave propagation.
12. Z. STRZYZAKOWSKI and L. ZIEMANSKI 1991 *Zeitschift für angewandte Mathematik und Mechanik* **71**, 221–224. On the application of the finite strips method to dynamical analysis of vehicle-track systems.
13. T. X. WU and D. J. THOMPSON 1998 Submitted to *Journal of the Acoustical Society of America*. Analysis of lateral vibration behaviour of railway track at high frequencies using a continuously supported multiple beam model.
14. N. VINCENT and D. J. THOMPSON 1995 *Vehicle System Dynamics* Supplement **24**, 100–114. Track dynamic behaviour at high frequencies. Part 2: experimental results and comparisons with theory.
15. M. A. HECKL 1995 *Acustica* **81**, 559–564. Railway noise—can random sleeper spacing help?
16. T. X. WU and D. J. THOMPSON 1999 *Journal of Sound and Vibration* **219**, 881–904. Effects of local preload on the foundation stiffness and vertical vibration of railway track.